Discrepancy in T_e Measurements of the Equatorial Ionosphere between ISR, SAMI2-PE and Satellite data

Sevag Derghazarian [1] David L. Hysell [1]

[1]Cornell University

Abstract

The Full Profile algorithm, based on ISR theory, provides complete altitude profiles of T_e up to plasmaspheric altitudes above Jicamarca, and is thus an invaluable tool in the study of the ionosphere.
However, challenges present in the inversion technique in longer pulse experiments causes T_e values to be significantly lower than those observed by DMSP satellites for a given altitude.
SAMI2-PE ionospheric model T_e values also present discrepancies with satellite data during sunrise and sunset times.
Efforts to address both the model and data processing deficiencies are explained.
In addition, a novel technique for correcting noise and lag product estimates based on order statistics is presented, which can be adapted to any ISR data contaminated by coherent echoes.

I. Introduction

Temperatures in the ionosphere and plasmasphere play a crucial role in the energetics and chemical composition of the upper atmosphere. T_e and T_i, being the only observable parameters in the energy balance of the thermosphere, are invaluable in our understanding of the ionosphere,(Rees,1989).

Previous studies uncovered discrepancies in T_e between ISR data and SAMI ionospheric models during sunrise, sunset and midday, where a temperature drop in the data was not present in the model outputs (Fig 1 and 2).

Figure 1 – Hybrid Pulse ISR Experiment, March 11-13, 2013, Jicamarca [1]

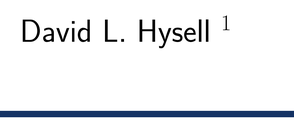

Figure 2 – SAMI2-PE T_e RTI Plot, March 11-13,2013 Jicamarca [1]

However, in the current study, ISR data from high altitude experiments and SAMI2-PE model output were both compared independently with DMSP satellite data, revealing significant differences.

II. Full Profile Algorithm: Forward Model

A combination of ISR and radar theory is involved in the construction of the forward model. The model inputs are T_e, T_i, N_e as well as H^+ and $He+$ fractions. The outputs are lag products. The difference between predicted and measured lag products is used to build the objective function we are looking to minimize.
Here is a visual schematic of the process:

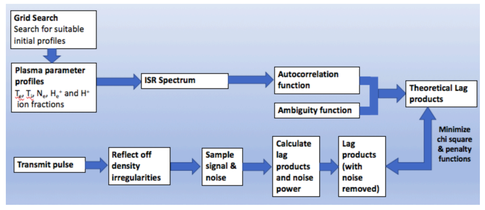

Figure 3 – Flow Chart Explaining Full Profile Algorithm

III. Challenge in Minimizing Objective Function

The forward model requires the computation of the plasma autocorrelation function, which is the inverse Fourier transform of the power spectrum and proportional to the expression:

$$\rho(k,\tau;r) \propto \mathcal{F}^{-1}\left[\frac{|\gamma_e|^2 Re(\sum_i^n (f_i\gamma_i)) + |\sum_i^n (f_i\gamma_i T_e/T_i) + i\lambda_d^2 k^2|^2 Re(\gamma_e)}{w|\gamma_e \sum_i^n (f_i\gamma_i T_e/T_i) + i\lambda_d^2 k^2|^2}\right] \quad (1)$$

where γ_e, γ_i are the complex admittances of the plasma. Lag products are then calculated from (1), using the equation:

$$<\mathrm{y}(\mathrm{t}_{s1}) y^*(t_{s2}) >= \int d\tau dr \rho(k,\tau;r) W_{t_{s1},t_{s2}}(\tau,r) \quad (2)$$

where W corresponds to the radar ambiguity function.
The function is intricate, with no indication it is convex. In the current code, a Levenberg-Marquart algorithm is employed for the nonlinear optimization, but the sensitivity to the initial guess makes it highly dependant on prior knowledge.

In addition, the inclusion of longer pulse lengths ($>$ 2ms) useful for probing higher altitudes, worsens the pathology, giving rise to a cost function more challenging to minimize. In the illustration below, one can see that with an improper guess, the algorithm can converge to any one of the local minimums.

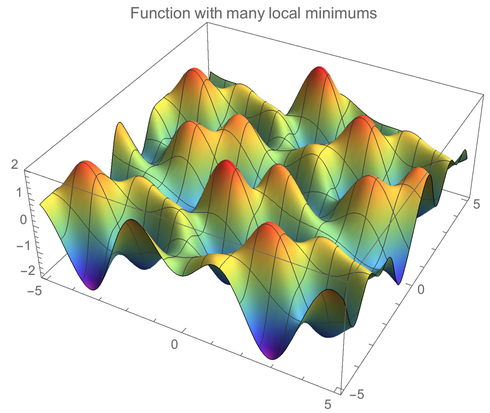

Figure 4 – Arbitrary Function with Multiple Local Minimums

The solution therefore to this challenge lies in the application of global optimization techniques for non-convex optimization functions. Currently, stochastic or partly stochastic techniques are being explored, such as Nelder-Mead (downhill simplex method), simulated annealing and genetic algorithms.

IV. Comparison of ISR, SAMI2-PE with DMSP satellite data

A high altitude ISR experiment was performed at Jicamarca from Jan 22 -25, 2019. A SAMI2-PE simulation was run for the same time period. Data was gathered from three different DMSP satellites (F15, F16, F17). The range of the DMSP data is $\approx$ 844 km, the magnetic latitude $\approx 1^o$, the longitude $282^o \pm 5^o$, and is available for six different local times indicated in the figures that follow.

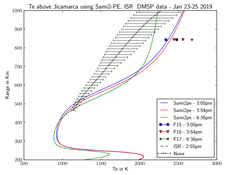

Figure 5 – Comparison of DMSP data with SAMI2-PE and ISR for Jan 22-25, 2019

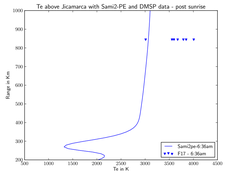

Figure 6 – Comparison of SAMI2-PE with DMSP data, Jan 22-25, 2019

It is important to bear in mind that satellite data can only validate SAMI2-PE and ISR data for a single or limited number of altitudes. For a more thorough comparison between physical data and model output over a large range of altitudes, the ISR inversion algorithm will need to be improved.

Figure 5 shows fairly good agreement of SAMI2-PE with satellite data in the mid and late afternoon (3pm and 3:54pm LT), with a deviation of at most 200K. The discrepancy is much larger however, around sunset time (6:36pm), with a value of around 700K. The same observation can be made in Figure 6, where a difference as high as 1000K is observed. The curves generated from ISR data appear to be around 700K lower than the corresponding T_e measured by F15.

These observations indicate that the onset of sunrise heating is later in the SAMI2-PE model than as measured in situ. This can be more clearly seen by looking at the presunrise period. Figure 7 shows values of $T_e \approx 1700K$ measured by the Hinotori satellite at $\approx$ 3:30am LT, whereas for the same time, values of $T_e < 900$K are obtained from SAMI2-PE simulations. This indicates the need for additional transport terms in SAMI2-PE, such as thermal diffusion across field lines.

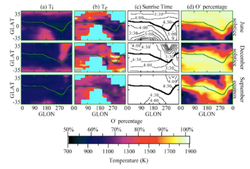

Figure 7 – T_e, T_i observed by Hinotori satellite from 1981-1982 for the presunrise period [2]

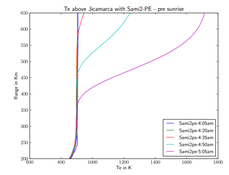

Figure 8 – SAMI2-PE presunrise temperatures, Dec 21 1982

V. Noise and Lag Product Expectation Correction Formulas

Formulas for correcting noise and lag product estimates were calculated from Jicamarca data. Order statistics is used to remove clutter from satellite echoes by throwing out voltage samples that lie on either end of an ordered list. Due to the skewness of the underlying distribution however, a bias is introduced in the expectation estimator, which requires a correction.

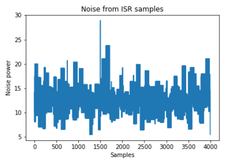

Figure 9 – Gaussian random noise from transmitter off period

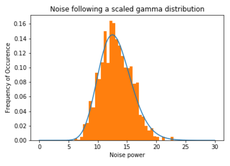

Figure 10 – Noise Power follows Gamma distribution

Correction Formula for Noise Power Expectation

$$\mu_{est} = Ae^{-bp} + C$$
$$C \approx \overline{X} - 0.316\theta_{est}e^{-7.06p}$$

In the first equation above, μ_{est} is the corrected expectation, $\overline{X}$ is the sample mean, θ_{est} is the estimated gamma scale factor by fitting, and p is the fraction of total samples thrown out from each side (ex: $\frac{2}{16}$).

Correction Formula for Lag Product Expectation

$$\mu_{est} = Ae^{-bp} + C$$
$$A = -(3.28\sigma - 1.6863)0.5688e^{(-1.306\rho)+0.5594}$$
$$b = 0.3436\rho + 6.7805$$
$$C = \overline{X}_{samp} - Ae^{(-b*p)}$$

In the first equation above, μ_{est} is the corrected expectation, p is the fraction of samples thrown out, ρ is the value of the correlation coefficient (taken from the measured ACF) between samples involved in the lag product.
The correction formulas above were found by first fitting a theoretical distribution to the chopped distributions created from ordered data, and then establishing a relationship between distributions. Below is a table that illustrates the effectiveness of the correction:

Error from chopped mean(%) - 1/4 removed	Error after correction (%)	Error from chopped mean - 1/2 removed	Error after correction (%)
1.33	0.07	1.75	0.04
1.24	0.03	1.78	0.04
1.36	0.07	1.86	0.09
1.39	0.09	1.89	0.12
1.23	0.07	1.66	0.12
1.34	0.01	1.88	0.06

Figure 11 – Accuracy of error correction formulas in recovering the true expectation of a test distribution

In summary, all three areas of improvement presented in the poster are being addressed simultaneously for improved data based and model generated values of the electron temperatures for any part of the day. The improvements to be made are:

Recommendations and Conclusions

- Determine an effective global optimization method to locate the global minimum in the objective function needed to fit ISR data and estimate values of T_e
- Incorporate additional transport terms to SAMI2-PE to resolve the discrepancies observed at sunrise and sunset.
- Add noise correction formulas to reduce the bias of the noise power and lag product estimators.

References

[1] Hysell et al. Topside equatorial ionospheric density, temperature, and composition under equinox, low solar flux conditions, *Journal of Geophysical Research*, 2015.

[2] C. K. Chao et al., Modeling the presunrise plasma heating in the lowâĂŘ to midlatitude topside ionospheres *Journal of Geophysical Research,*, *115*, 2010.

[3] J.E. Pingree, Incoherent Scatter Measurements and Inferred Energy Fluxes in the Equatorial F-Region Ionosphere*Doctoral Dissertation, Cornell University, 1990.*